

### **Re-crystallization experiments**

A crystallization protocol was developed based on Fel solubility data. The selected solvents were maintained at boiling temperature. Slightly excess amount of Fel was dissolved in 4 ml of solvent. Super-saturation was achieved through decreasing the solubility of the drug by addition of an anti-solvent that induced crystallization of the drug. Selected anti-solvent (1 ml) was added in the crystallization medium. The solutions were filtered into a crystallization vessel and allowed to cool to achieve super-saturation. The evaporation rate was controlled using an inverted cotton plugged funnel. After 24h, crystals were collected, dried and stored until further use.

### **Solid state characterization**

**Microscopy** - Fel crystals inspection and analysis was carried out using inverted microscope coupled with NIE software (Nikon TiU). The particle sizes and average aspect ratios were determined (n=100). The aspect ratio, which is defined as the ratio of the maximum to the minimum diameter of the particle, was used as a shape parameter for the crystals.

**Thermal characterization** - Differential scanning calorimetry (DSC) analysis of plain Fel and Fel crystals was carried out using Mettler Toledo DSC system. Indium was used for calibration. The sample cell was purged with dry nitrogen at a flow rate of 80 mL/min. Accurately weighed samples (~5 mg) in aluminium crimped pans with a pinhole were scanned at a heating rate of 10 °C/min over a temperature range of 25-200 °C. Presence of any solvent/degradation during heating was examined by thermo-gravimetric analysis (TGA) using (Universal, V47A, TA instruments), on accurately weighed (5-10 mg) samples loaded in alumina crucibles that were heated at a rate of 10 °C/min over a temperature range of 25 to 300 °C under dry nitrogen purge of 60 mL/min.

**Powder X-ray diffraction (PXRD)** - PXRD patterns of samples were obtained at room temperature on a X-ray powder diffractometer (X'Pert Pro PANalytical), using Ni-filtered Cu K<sub>α</sub> radiation (wave length=1.5406Å). The data was recorded over a scanning 2θ range of 2° to 50° at a step time of 0.045 steps/0.5 sec.

***X-ray Photoelectron Spectroscopy (XPS)*** - XPS studies were performed using KRATOS-AXIS 165 microprobe system model, using Al-K $\alpha$  radiation of 250 W X-ray tube as a radiation source with energy of 1486.6 eV, 16 mA  $\times$  12.5 kV under working pressure lower than  $1 \times 10^{-8}$  Nm $^{-2}$ . Binding energy range was from 0 to 1100 eV for regions of C 1s, N 1s, O 1s, and Cl 2p with an average peak binding energy of 286.0, 400.9, 533.0, and 200.2 eV respectively. All spectra were corrected for baseline and fitted using Gaussian function. The fitting of the XPS curves was analyzed with VISION-2 software. Surface atomic concentration was determined from integrated peak intensities and the corresponding relative sensitivity factor.

### ***In vitro* dissolution studies**

All re-crystallized samples were passed through BSS sieve no. 10 and 12, without breaking or crushing the samples. The crystals which passed through sieve no. 10 but retained on sieve no. 12 (10/12), were weighed and subjected to particle size measurement by microscopy. The particle size was reported in terms of 10 (D $_{10}$ ), 50 (D $_{50}$ ), and 90 (D $_{90}$ ) percent cumulative percentage undersize (supplementary table 1). These crystals were then used for dissolution study to exclude the impact of particle size on dissolution rate. Dissolution testing was carried out in an USP Apparatus II at a rotational speed of 50 rpm (n=3). Weighed quantity of crystals (20 mg) was added to the dissolution medium (0.1% v/v SLS in distilled water). Samples were withdrawn at regular intervals through a syringe connected to a membrane filter (0.45  $\mu$ m). Equal quantity of fresh dissolution medium was immediately replaced. These samples were then evaluated for drug concentration at a  $\lambda_{\text{max}}$  238 by UV method.

## **In vivo pharmacokinetic studies**

**Dosing protocol-** Female SD rats (2–3 months of age, 200–250 g) were housed according to the CPCSEA guidelines in the Central Animal Facilities of the NIPER, Hyderabad. These facilities have obligatory accreditation of the authorized CPCSEA. Approval for animal study was granted by the Institutional Ethical Committee for Animal Experimentation (IAEC approval No. NIP/03/2014/PE/83). Prior to oral drug administration, two groups of rats ( $n = 6$ ) were fasted overnight ( $>12$  h). For comparison of pharmacokinetic parameters, selected crystals and free drug were given to the rats via oral gavage (10 mg/kg). Blood samples (0.5 ml) were collected from the retro orbital plexus at time points 0.25, 0.5, 1, 2, 4, 6, 8 and 12 h after dosing. Immediately plasma was harvested by centrifugation at 3500 g for 5 min and transferred to a fresh eppendorf tube containing 30  $\mu$ l of heparin and frozen to  $-20^{\circ}\text{C}$  prior to analysis.

**Extraction and quantification of Fel in plasma samples** - To 100  $\mu$ l of plasma, 25  $\mu$ l of internal standard (Lacidipine) was added and vortexed for 60 s. Then, 375  $\mu$ l of methanol was added to precipitate proteins, vortexed for 5 min and centrifuged at 5000 g for 10 min. Supernatant (100  $\mu$ l) was taken, filtered and analyzed for drug content by validated RP-HPLC method. The HPLC system (e2695 Waters) consisted of an HPLC pump, automated injector equipped with a UV detector (2998 PDA). Calibration curves were designed over the concentration range of 10-1000 ng/ml ( $r^2$  0.997) and were used for the conversion of the Fel/Lacidipine chromatographic area to the concentration of Fel. Mobile phase employed for analysis was acetonitrile and 10 mM ammonium acetate phosphoric acid solution (65:35). Retention time of Fel and internal standard was found to be 5.4 and 9.2 min respectively. The detection wavelength set for Fel was at 238 nm and the column was maintained at  $25^{\circ}\text{C}$ .

**Pharmacokinetic data analysis** - The plasma concentration time data was analyzed by one compartmental model, using demo version of Kinetica software (Thermo scientific). Required pharmacokinetic parameters like total area under the curve  $(\text{AUC})_{0-12}$ , terminal phase half life ( $t_{1/2}$ ), peak plasma concentration ( $C_{\text{max}}$ ) and time to reach the maximum plasma concentration ( $T_{\text{max}}$ ) were determined. The relative bioavailability of selected Fel crystals after oral administration was calculated in comparison to Fel suspension.

## Computer simulation studies

Fel crystallographic information file (CSD code DONTIJ) was taken from Cambridge Structure Database with the following cell parameters: Symmetry: Monoclinic  $P2_1/c$ , a: 12.086, b: 12.077, c: 13.425,  $\alpha$ : 90,  $\beta$ : 116.13,  $\gamma$ : 90.<sup>11</sup> All molecular dynamics and morphology simulations were executed using Materials Studio 6.1. Geometry optimization was carried out using forcite algorithm (COMPASS force field). Face list was created using morphology module, which gave hkl and  $d_{hkl}$  values of all important facets. Modelling method for crystal morphology calculation was based on modified attachment energy method.

### Generation of morphology from calculated modified attachment energy

The surface docking method as a prediction tool was employed to simulate the impact of solvents and anti-solvents on the crystal morphology. For the solid surface preparation, the crystal morphology was computed using AE (attachment energy) and the MI (morphologically important) facets were determined. The AE method generated possible crystal faces which controlled the morphology. These MI facets were picked individually and provided the required lattice values for amorphous cell generation. Fel crystal was sliced parallel to their respective hkl plane. A crystal slice was prepared as a periodic superstructure (8 molecules). This crystal slice was optimized by the MD (molecular dynamics). An amorphous cell was created, which enclosed calculated number of solvent and anti-solvent molecules. Amorphous cell for Fel-1 included 200 molecules of acetonitrile whereas amorphous cell for Fel-2 included 150 molecules of ethanol and 50 molecules of hexane. The amorphous cell was further refined by MD technique. The following task involved optimization of amorphous cell. This amorphous cell was then minimized at 10,000 iteration steps. The following equilibration on this cell comprised of 100 ps NVE (N-constant number of particles, V-constant volume, E-constant energy) and 10 ps NPT runs (N-constant number of particles, P-constant pressure, T-constant temperature). Layer docking interfacial method was used for MD calculation to study the impact of the solvent/anti-solvent on the crystal habit. One part of this model was the crystal segment and the solvent layer occupied another. The energy minimization was carried out before the MD simulation. NVT calculations were carried out for 10 ps with a time step of 1 fs. The attained PE (potential energy) was denoted as  $E_{total}$ . Consequently, the energies of the separated structures of

the crystal surface and amorphous layer were determined and denoted as  $E_{\text{surface}}$  and  $E_{\text{amorphous}}$  correspondingly.

For the equilibration stage, the time step for the MD simulation was fixed with defined period (10ps). After equilibrating the system, the production stage was performed. The Coulombic and van der Waals interactions were calculated by employing the standard Ewald summation method to determine the potential-energy calculations. Modified attachment energy (MAE) was then calculated by formula: <sup>14, 33, 35, 36</sup>

$${}^{\text{mod}}E_{\text{att}} = E_{\text{total}} - (E_{\text{surface}} + E_{\text{amorphous}})$$

where  ${}^{\text{mod}}E_{\text{att}}$  represents the modified attachment energy of selected solvent with specific crystal face and  $E_{\text{total}}$  represents the minimized energy of layer.  $E_{\text{surface}}$  represents the energy of sliced crystal surface from layer and  $E_{\text{amorphous}}$  represents the energy of sliced solvent surface from layer. The modified habit was generated based on the relation stated by Hartman and Bennema.<sup>36</sup>

$$R_g \sim [{}^{\text{att}}E_{\text{mod}}]$$

Where  $R_g$  represents the growth rate in a particular direction, which is directly proportional to the modified attached energy. Morphology tool of Material Studio 6.1 was employed for the prediction of the morphology in presence of the given solvent.

### **Hirshfeld surface analysis**

Hirshfeld surface analysis of intermolecular interactions in each phase was performed using Crystal Explorer (Version 3.0). Hirshfeld surfaces Analysis is found to be a valuable tool for explanation of intermolecular contacts in molecular crystals. The technique has been used for various other solid state forms of APIs like co-crystals, polymorphs etc.<sup>23</sup> However, authors are using that first time for studying crystal growth pattern. The Hirshfeld surfaces and relative 2-D fingerprint plots are particularly supportive for studying important intermolecular contacts of Fel with their medium (solvent/anti-solvent).

**Supplementary table 1.** hkl,  $d_{hkl}$ , % total facet area (TFA), attachment energy, surface energy and modified attachment energy of Fel by different models

		Vacuum morphology (%TFA)			%TFA by Modified attachment energy (MAE) method	
hkl	$d_{hkl}(\text{Å})$	BFDH	GM (attachment energy)	EM (surface energy)	Fel-1	Fel-2
{ 1 0 0}	10.85	26.49	32.95 (-55.35)	17.69 (0.170)		
{ 0 1 1}	8.53	37.48	43.56 (-56.94)	28.95 (.138)	7.17 (-82.04 )	
{ 1 1 0}	8.07	9.24	3.11 (-77.19)		25.55 (-75.59 )	57.90 (-83.15 )
{ 1 1 -1}	8.03	21.69	17.50 (-71.73)	11.32 (0.164 )	39.25 (-36.59 )	0.58 (-89.46 )
{ 1 0 -2}	6.65	5.05	2.72 (-85.39 )	6.10 (0.164 )	19.89 (-71.59)	31.40 (-106.52 )
{ 0 2 0}	6.03	0.02	0.14 (-86.68)	7.68 (0.154)	8.12 (-77.6 )	10.10 (-86.15 )
{ 2 1 -1}	5.40			9.48 (0.176)		

**Supplementary table 2.** Fel re-crystallization with screened solvents, solvents/anti-solvent

Anti-solvent	Solvent	Solubility (mg/ml)	Crystal habit	Average aspect ratio $\pm$ SD
	Acetone	265	Plates (non-uniform)	
	Ethanol	130	Plates	3.46 $\pm$ 1.02
	Methanol	60	Plates	2.58 $\pm$ 0.87
	<b>Acetonitrile</b>	<b>170</b>	<b>Thick plates/ Rhombohedral</b>	<b>1.15 <math>\pm</math> 0.14</b>
Hexane	Acetone		Thin plates	
	<b>Ethanol</b>		<b>Thick plates</b>	<b>1.37 <math>\pm</math> 0.24</b>
	Methanol		Plates (non-uniform)	1.89 $\pm$ 0.62
	Acetonitrile		Thin plates	1.92 $\pm$ 0.46
IPA	Acetone		Thin plates	
	Ethanol		Plates (non-uniform)	1.78 $\pm$ 0.27
	Methanol		Plates (non-uniform)	2.32 $\pm$ 1.61
	Acetonitrile		Thin plates	2.43 $\pm$ 0.72

All values are expressed as mean  $\pm$  SD (n=100), precipitation was observed with chloroform, ethyl acetate and DCM

**Supplementary table 3. Surface chemistry of fel facets**

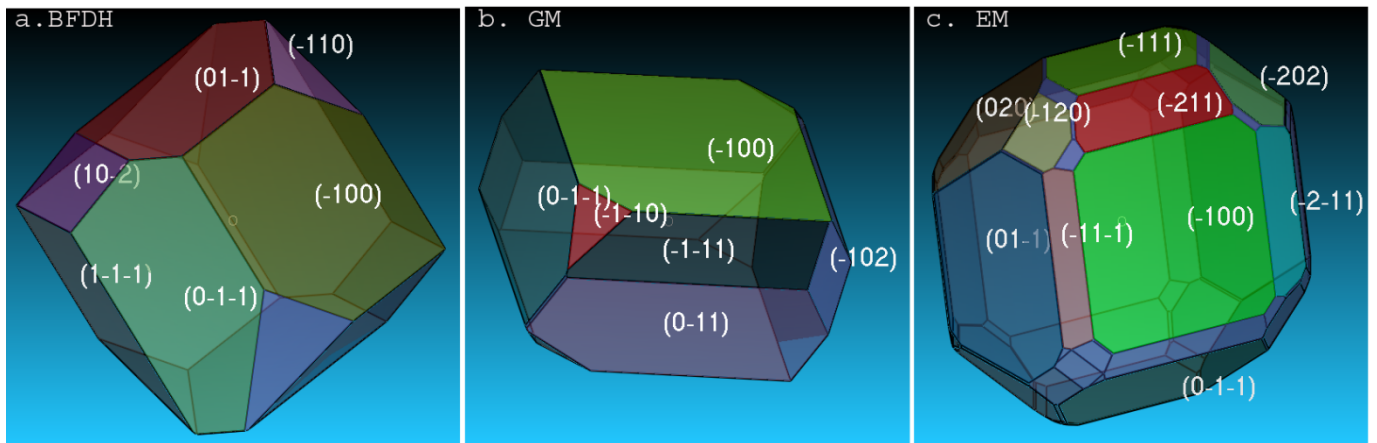
Number of functional groups exposed to crystal surface				
Hkl	CH <sub>3</sub>	CO/COO	Cl	Aromatic ring
{ 1 0 0}	2	2		
{ 0 1 1}	1		1	
{ 1 1 0}	5	2	1	
{ 1 1 -1}	1	2	1	1
{ 1 0 -2}	2	1		
{ 0 2 0}	2			

**Supplementary table 4.** Particle size distribution of Fel crystals

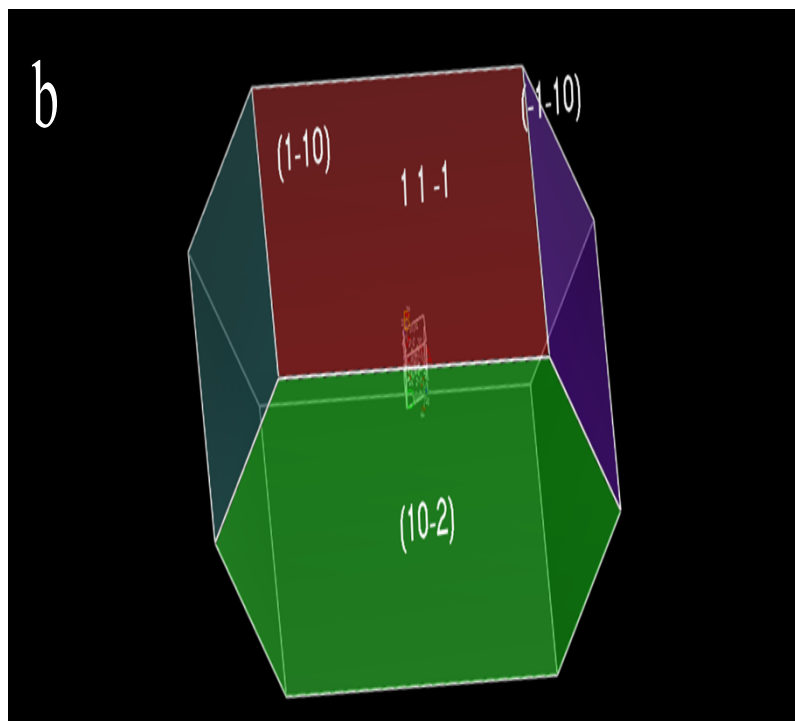
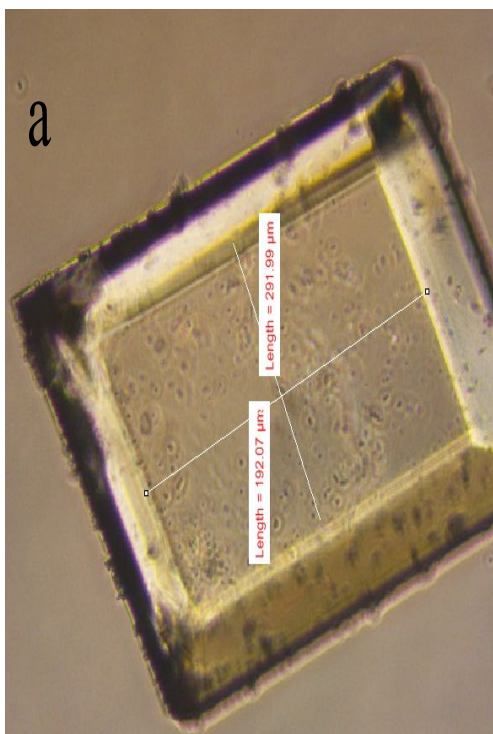
	$D_{10}$ ( $\mu\text{m}$ )	$D_{50}$ ( $\mu\text{m}$ )	$D_{90}$ ( $\mu\text{m}$ )
Fel-1	1149.28	1280.5	1452.22
Fel-2	1148.24	1305.34	1478.54

**Supplementary table 5.** Dissolution parameters of plain Fel and re-crystallized Fel

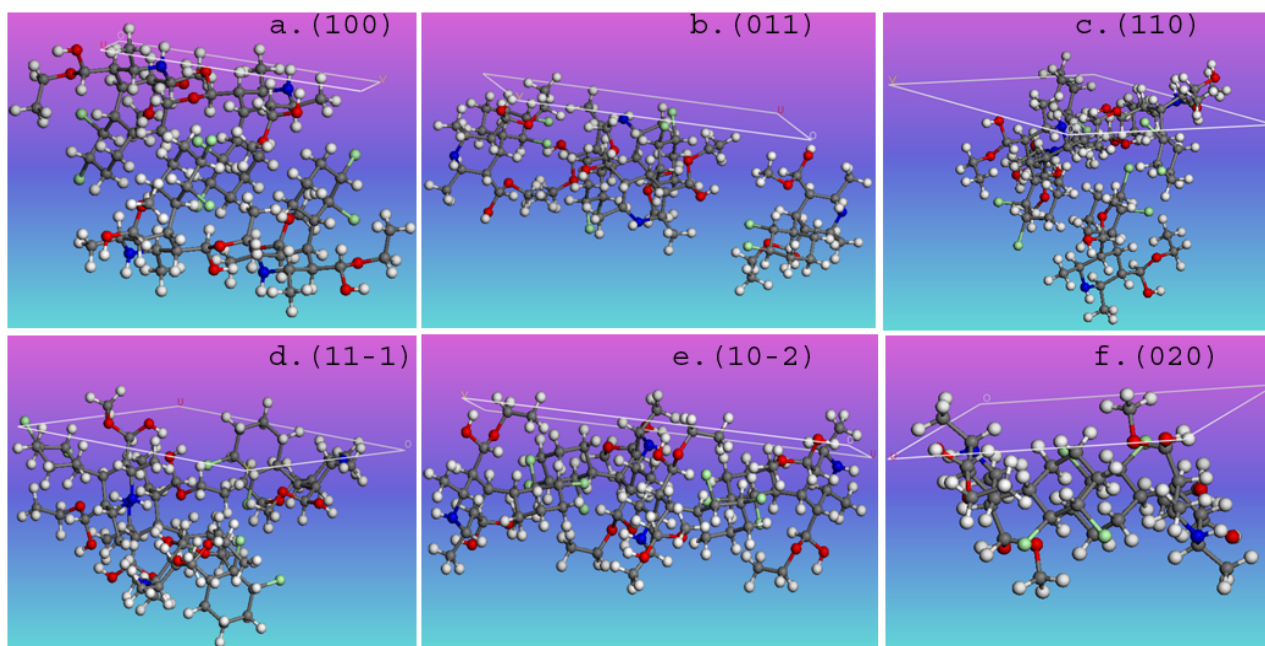
	$DE_{60}$	$DE_{180}$	$DE_{360}$
Fel	7.5	11.9	17.2
Fel-1	10	31.2	44.9
Fel-2	8.3	21.1	30.7



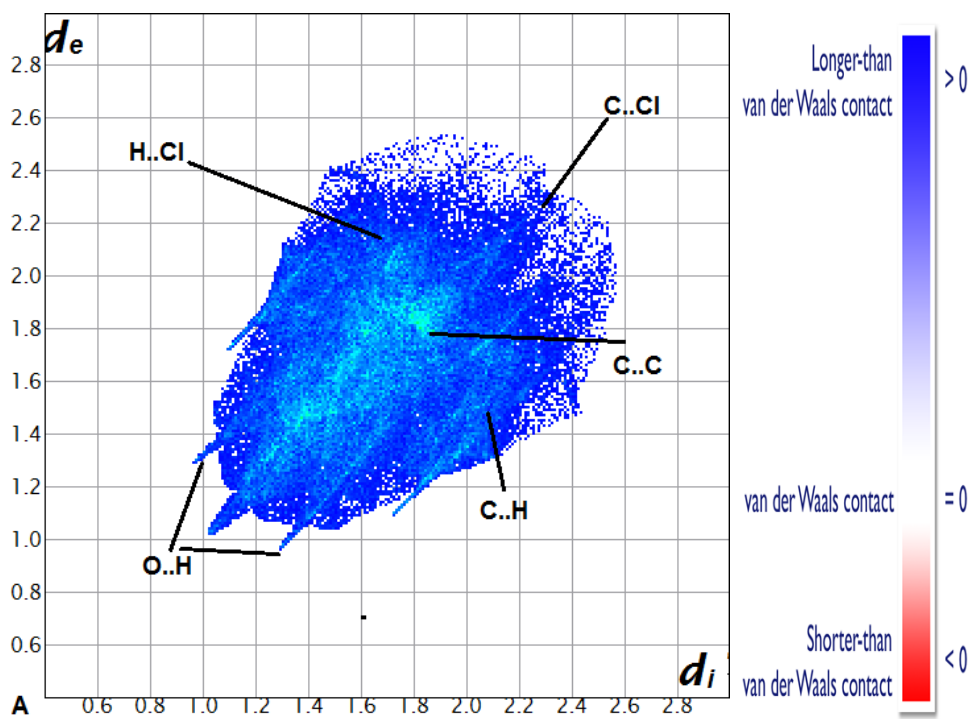
**Supplementary figure 1.** Vacuum morphology of Fel a. BFDH, b. Morphology growth, c. Equilibrium morphology



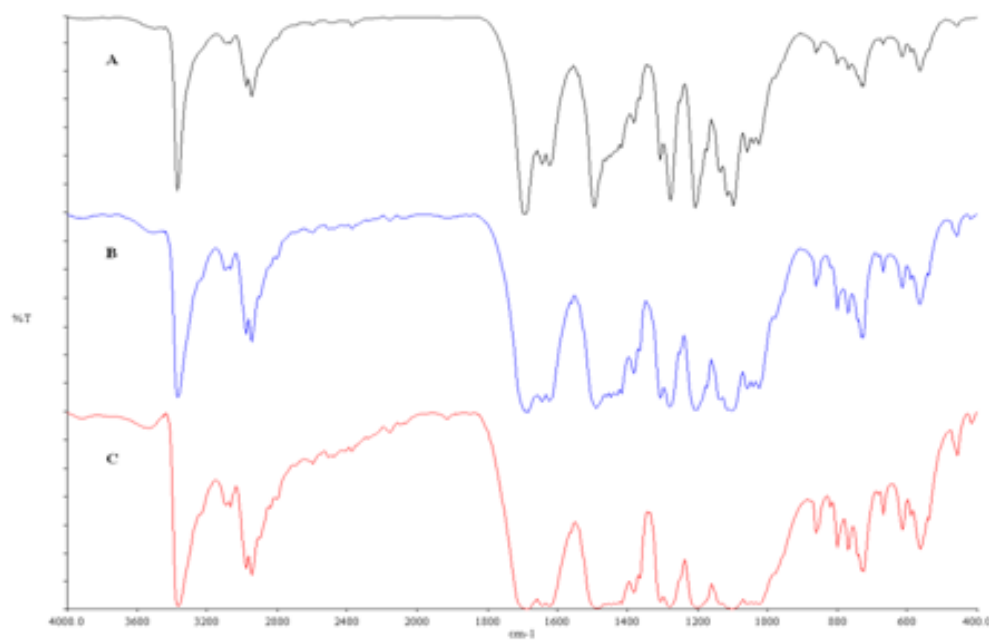
**Supplementary figure 2.** a. Experimental morphology of Fel-1, b. Simulated morphology of Fel-1



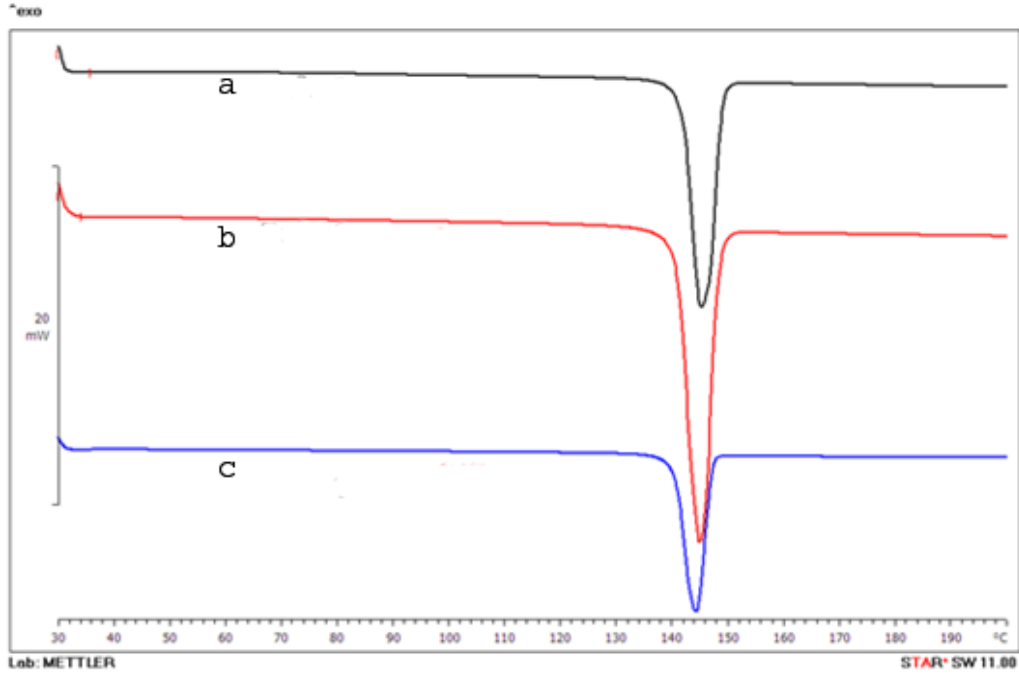
**Supplementary figure 3.** Crystal slices of different facets of Fel expressing the presence of polar and non-polar functional groups



**Supplementary figure 4.** Fingerprint plots generated from Hirshfeld surface analysis of the Fel form I (CSD code DONTIJ)

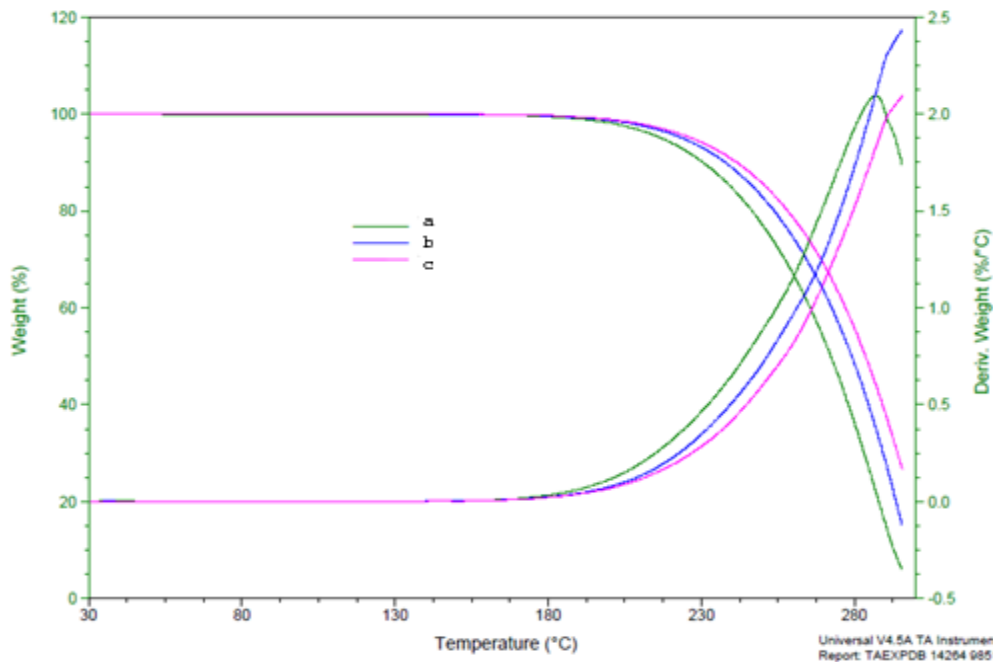


**Supplementary figure 5.** FTIR of selected Fel crystals a. Fel b. Fel-1 c. Fel-2



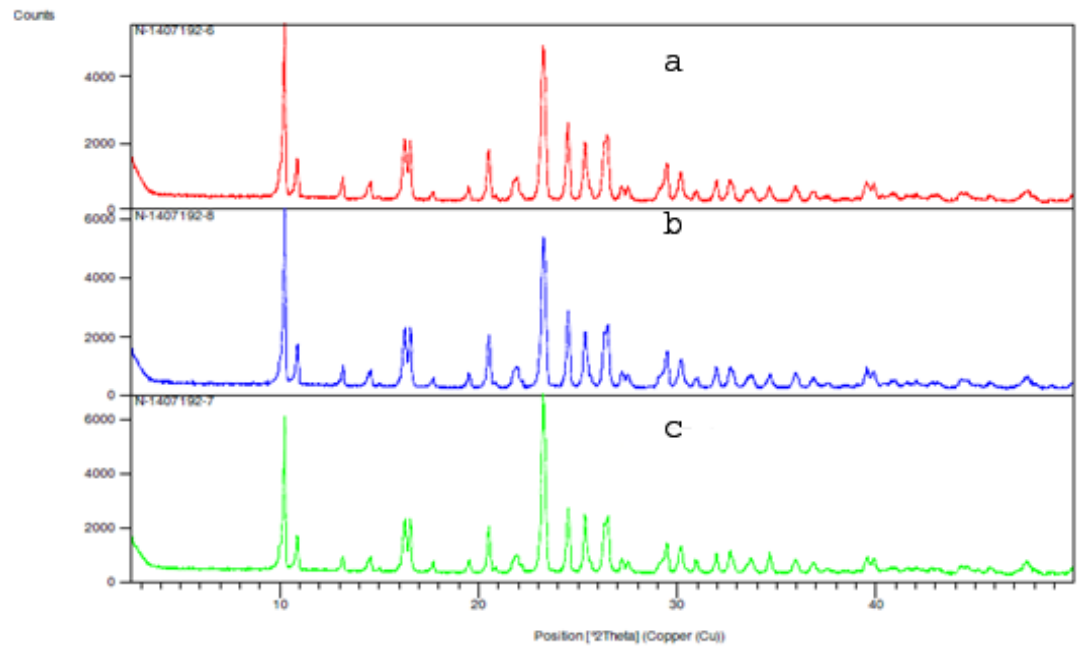
Suppleme

ntary figure 6. DSC curves of selected Fel crystals a. Fel b. Fel-1 c. Fel-2



Supplem

entary figure 7. TGA curves of selected Fel crystals Fel, Fel-1 and Fel-2



**Supplementary figure 8.** PXRD of selected Fel crystals a.Fel,b. Fel-1,c. Fel-2